Figure S1

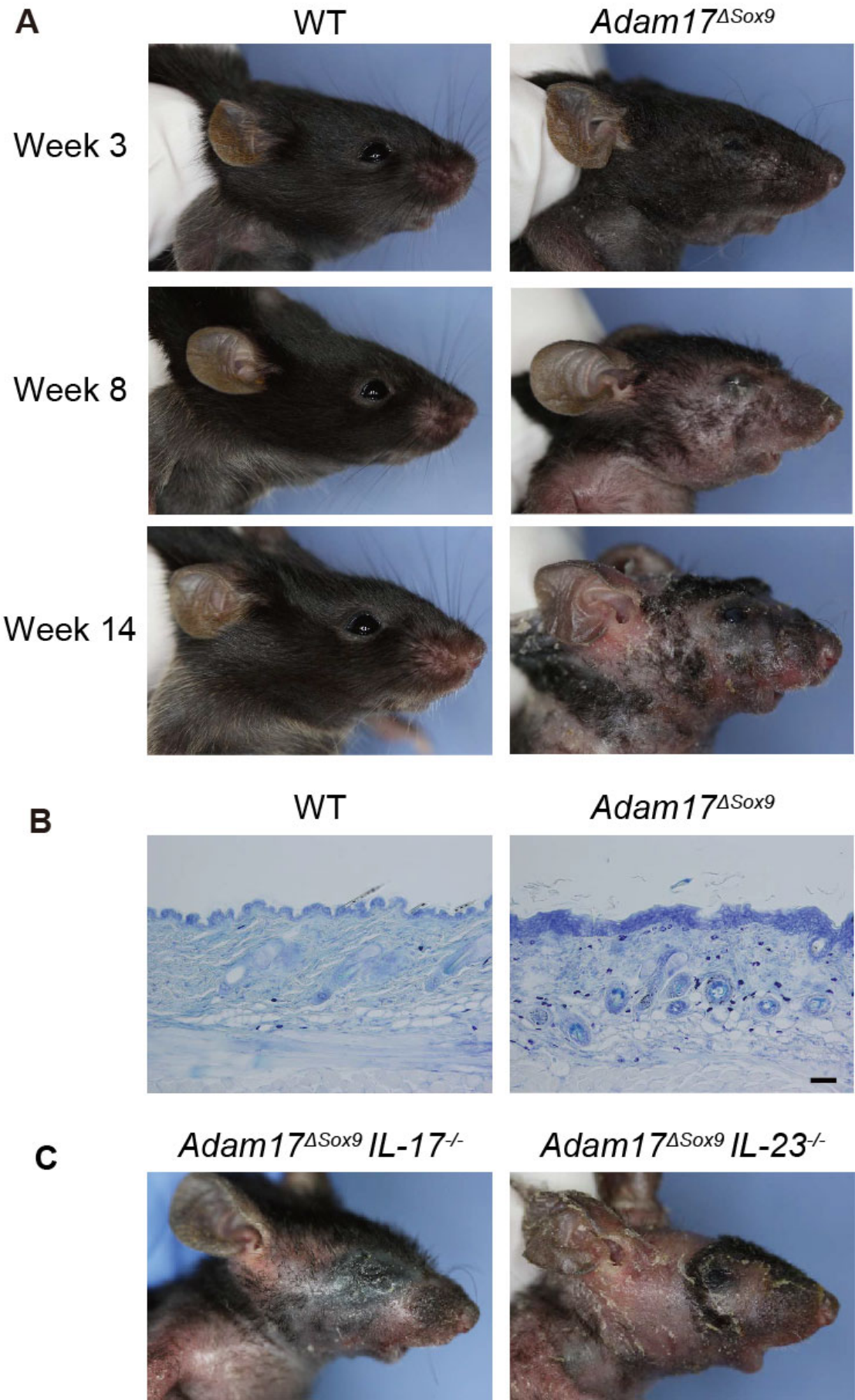
A
WT
Adam17ΔSox9
Week 3
Week 8
Week 14
B
WT
Adam17ΔSox9
C
Adam17ΔSox9 IL-17-/-
Adam17ΔSox9 IL-23-/-

Figure S2

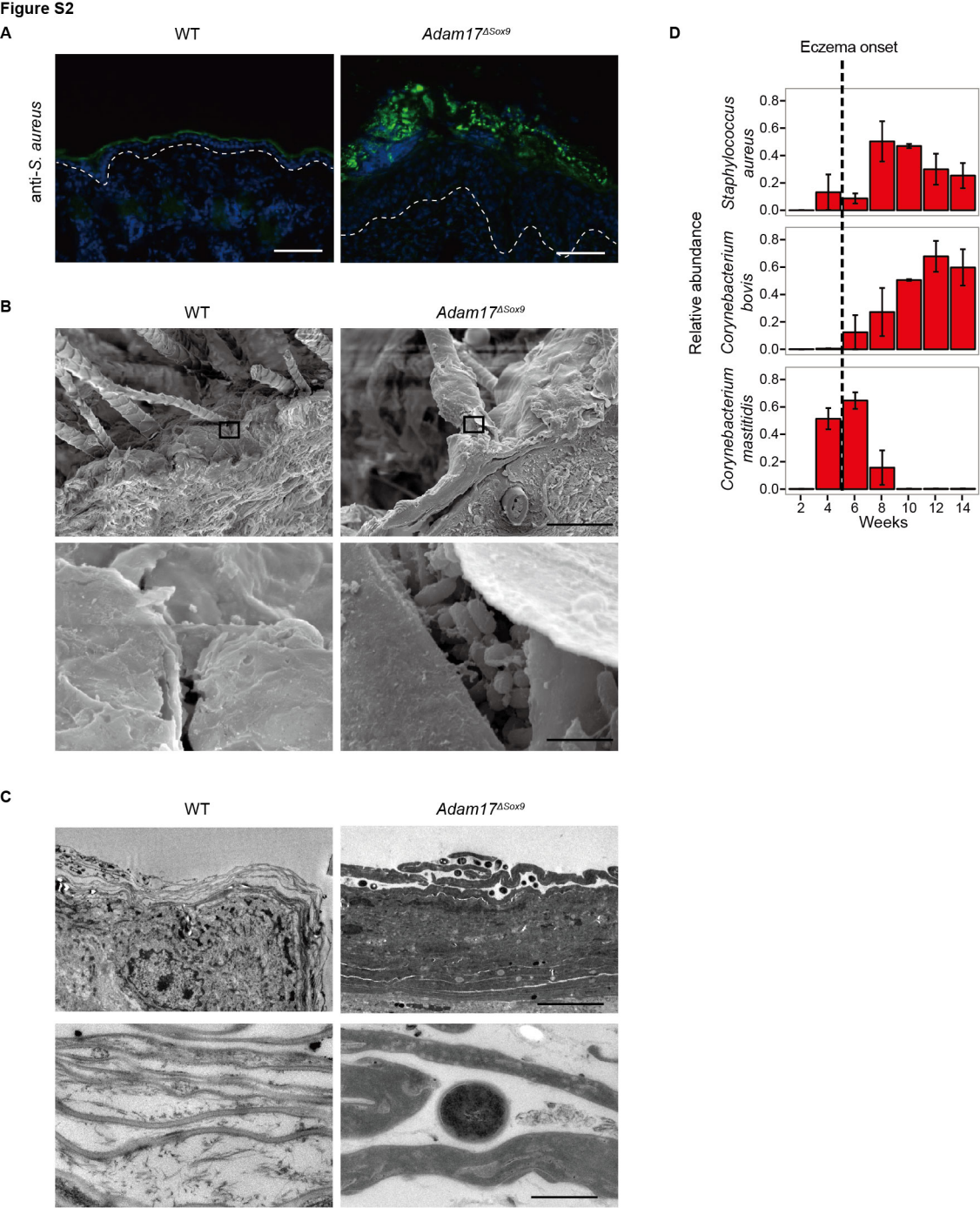
A
WT
Adam17ΔSox9
anti-S. aureus
B
WT
Adam17ΔSox9
C
WT
Adam17ΔSox9
D
Eczema onset
Relative abundance
Staphylococcus aureus
Corynebacterium bovis
Corynebacterium mastitidis
0.0
0.2
0.4
0.6
0.8
2
4
6
8
10
12
14
Weeks

Figure S3

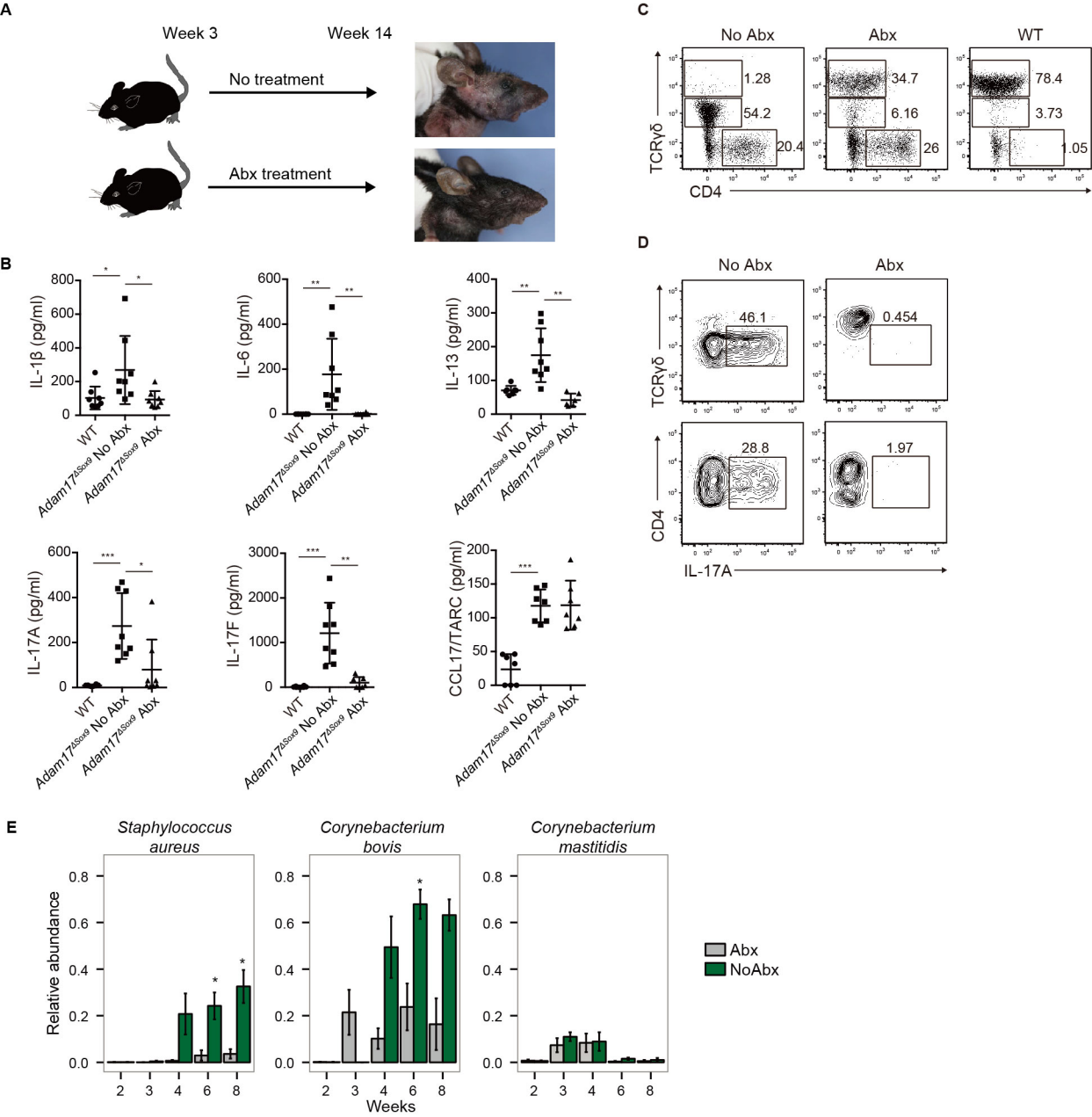
A
Week 3
Week 14
No treatment
Abx treatment
B
IL-1β (pg/ml)
IL-6 (pg/ml)
IL-13 (pg/ml)
IL-17A (pg/ml)
IL-17F (pg/ml)
CCL17/TARC (pg/ml)
WT
Adam17ΔSox9 No Abx
Adam17ΔSox9 Abx
C
No Abx
Abx
WT
TCRγδ
CD4
1.28
54.2
20.4
34.7
6.16
26
78.4
3.73
1.05
D
No Abx
Abx
TCRγδ
CD4
IL-17A
46.1
0.454
28.8
1.97
E
Staphylococcus aureus
Corynebacterium bovis
Corynebacterium mastitidis
Relative abundance
Weeks
Abx
NoAbx

Figure S4

A

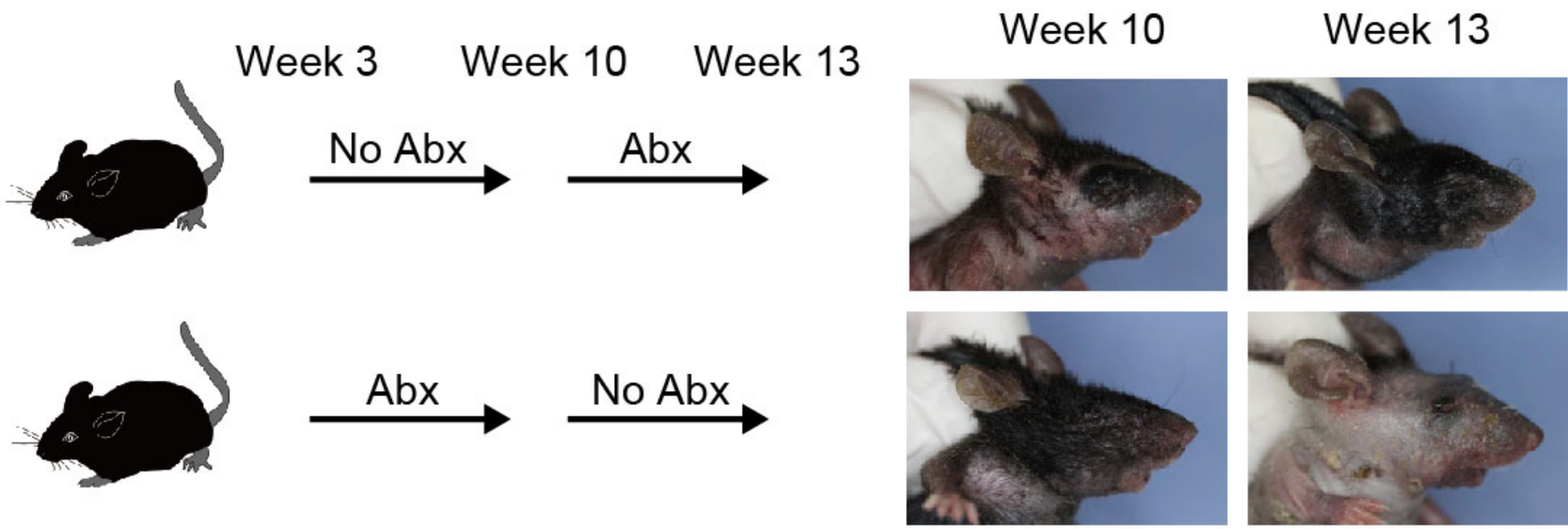
Week 3
Week 10
Week 13
No Abx
Abx
Abx
No Abx
Week 10
Week 13

B

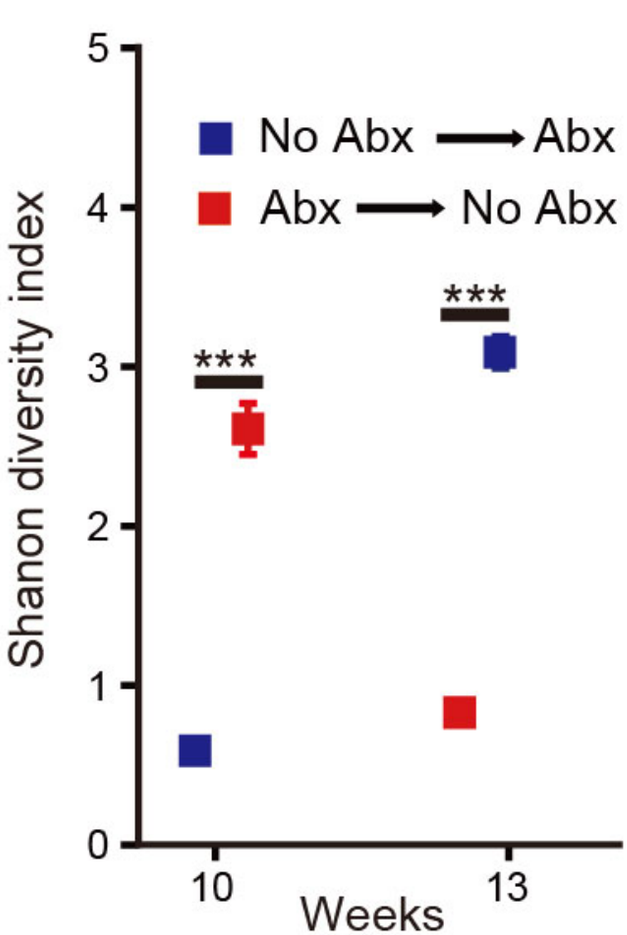
5
4
3
2
1
0
No Abx → Abx
Abx → No Abx
***
***
Shanon diversity index
10
13
Weeks

Figure S5

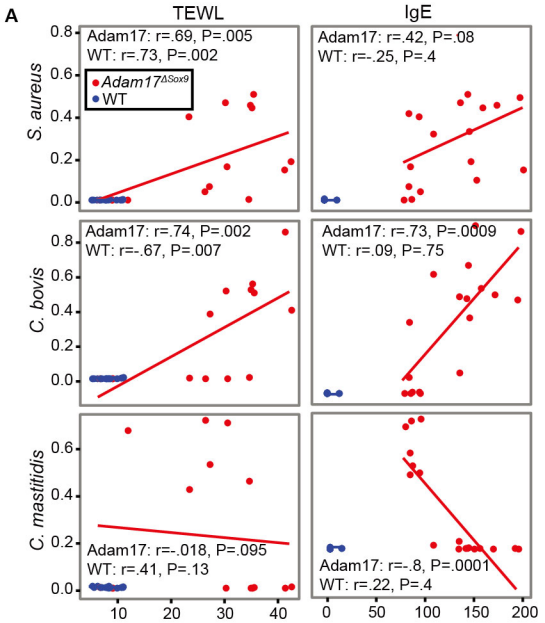
A
TEWL
IgE
S. aureus
C. bovis
C. mastitidis
Adam17: r=.69, P=.005
WT: r=.73, P=.002
Adam17ΔSox9
WT
Adam17: r=.42, P=.08
WT: r=-.25, P=.4
Adam17: r=.74, P=.002
WT: r=-.67, P=.007
Adam17: r=.73, P=.0009
WT: r=.09, P=.75
Adam17: r=-.018, P=.095
WT: r=.41, P=.13
Adam17: r=-.8, P=.0001
WT: r=.22, P=.4

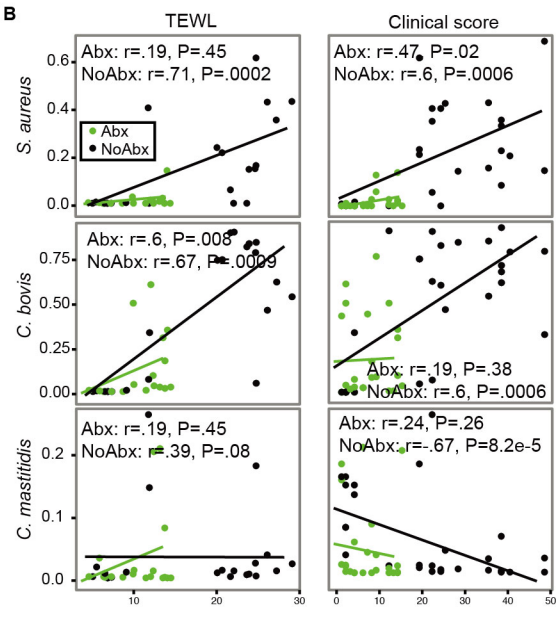
B
TEWL
Clinical score
S. aureus
C. bovis
C. mastitidis
Abx: r=.19, P=.45
NoAbx: r=.71, P=.0002
Abx
NoAbx
Abx: r=.47, P=.02
NoAbx: r=.6, P=.0006
Abx: r=.6, P=.008
NoAbx: r=.67, P=.0009
Abx: r=.19, P=.38
NoAbx: r=.6, P=.0006
Abx: r=.19, P=.45
NoAbx: r=.39, P=.08
Abx: r=.24, P=.26
NoAbx: r=-.67, P=8.2e-5

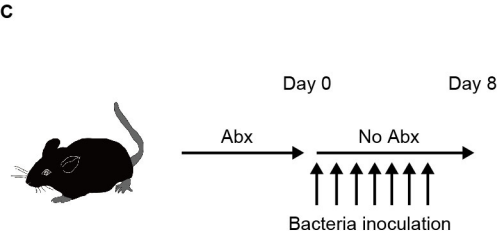
C
Day 0
Day 8
Abx
No Abx
Bacteria inoculation

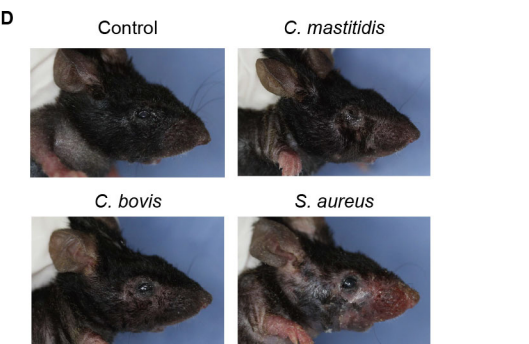
D
Control
C. mastitidis
C. bovis
S. aureus

Figure S6

WT

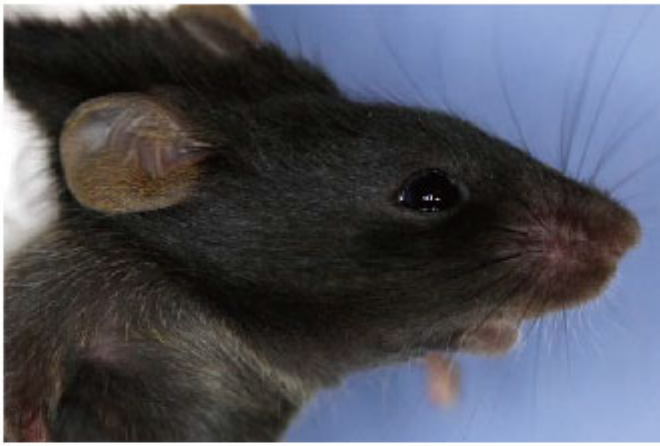

Egfr$^{\Delta Sox9}$

Figure S7

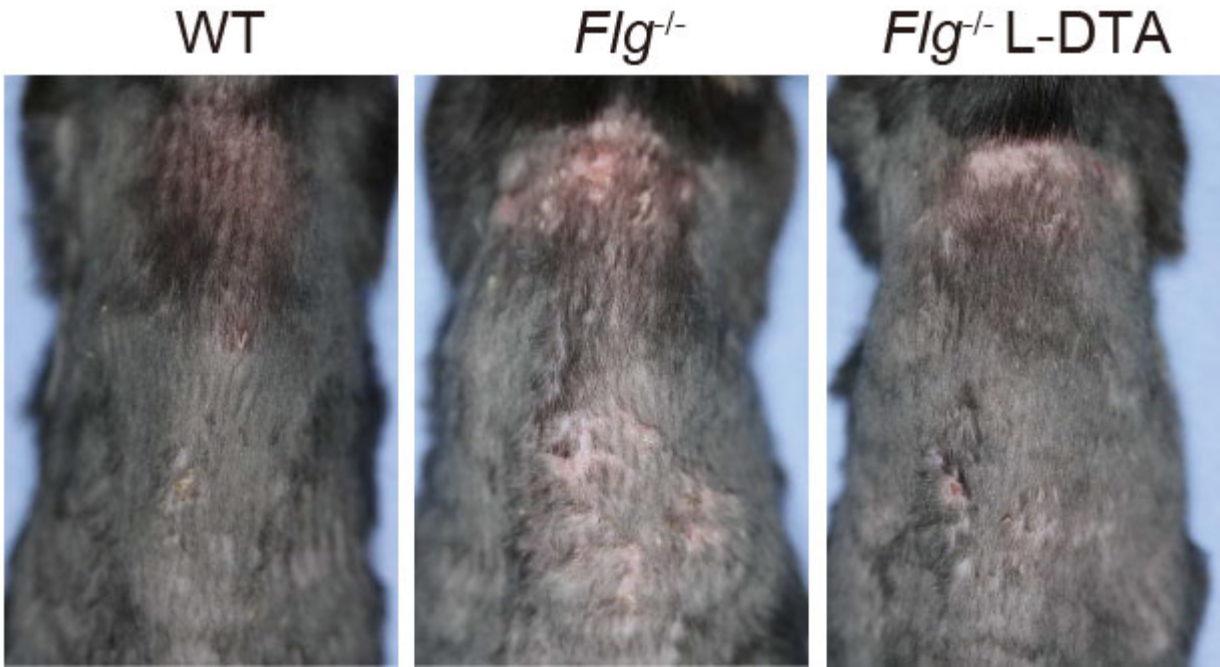

Supplemental Figure legends

Figure S1. *Adam17*$^{\Delta Sox9}$ mice develop eczematous dermatitis independent of IL-17 and IL-23. Related to Figure 1.
(A) Onset of eczematous dermatitis in *Adam17*$^{\Delta Sox9}$ mice. Gross phenotype at indicated time points after birth. (B) Toluidine blue staining (positive cells reflect mast cells) of WT and *Adam17*$^{\Delta Sox9}$ mouse skin. Scale bars, 50 μm. (C) 8-week-*Adam17*$^{\Delta Sox9}$ mice in *Il17*-/- or *Il23*-/- background.

Figure S2. *S. aureus* colonization in *Adam17*$^{\Delta Sox9}$ mouse skin. Related to Figure 2.
(A) Immunofluorescence microscopy of *S. aureus* as detected by anti-*S. aureus* antibody (green) and Hoechst (blue) in the stratum corneum of *Adam17*$^{\Delta Sox9}$ mouse skin. White dashed lines indicate basement membrane. Scale bars, 50 μm. (B) Scanning electron microscopy on skin surface of WT and *Adam17*$^{\Delta Sox9}$ mice. Note the presence of bacteria around hair follicles. Round bacteria represent *S. aureus* and oval bacteria *Corynebacterium* spp. Lower panels represent higher magnification of the squared areas in the upper panels. Scale bars, 50 μm (upper panels), 1.5 μm (lower panels). (C) Transmission electron microscopy of ultra-thin skin sections from WT and *Adam17*$^{\Delta Sox9}$ mice. Scale bars, 5 μm (upper panles), 0.5 μm (lower panels). (D) Dysbiotic changes in *Adam17*$^{\Delta Sox9}$ mice. Relative abundance of 16S rRNA gene sequences of *S. aureus*, *C. bovis* and *C. mastitidis* in *Adam17*$^{\Delta Sox9}$ mice at indicated time points. Data are shown as mean ± SEM. The dashed line indicates onset of eczema in these mice.

Figure S3. Changes in cytokine expression and the dysbiotic flora in antibiotics-treated *Adam17*$^{\Delta Sox9}$ mice. Related to Figure 3.
(A) *Adam17*$^{\Delta Sox9}$ mice were either treated or left untreated with an antibiotic cocktail since 3 weeks after birth. Shown are representative gross phenotypes of mice at week 14. (B) Serum levels of IL-1β, IL-6, IL-13, IL-17A, IL-17F and CCL17/TARC in WT, *Adam17*$^{\Delta Sox9}$ and antibiotics-treated *Adam17*$^{\Delta Sox9}$ mice (N=8). (C) Numbers of epidermis-infiltrating T cells in antibiotic-treated and non-treated *Adam17*$^{\Delta Sox9}$ mice analyzed via flow cytometry (N=7) and (D) IL-17A- producing γδ T cells and CD4 T cells (N=7). (E) Relative abundance of 16S rRNA gene sequences of *S. aureus*, *C. bovis* and *C. mastitidis* of antibiotic-treated and untreated *Adam17*$^{\Delta Sox9}$ mice at indicated time points. Data are shown as mean ± SEM. *P<0.05, **P<0.01 as determined by Student's *t* test.

Figure S4. Antibiotic treatment normalizes dysbiosis and rescues eczematous phenotype in *Adam17*$^{\Delta Sox9}$ mice. Related to Figure 4.
(A) Crossover of antibiotics treatment protocol. A group of *Adam17*$^{\Delta Sox9}$ mice were left untreated from 3~9 weeks after birth, and were then put on antibiotics from 10~13 weeks, or vice versa. Right panels show phenotypic changes in *Adam17*$^{\Delta Sox9}$ mice during the crossover protocol at indicated time points. The same mice are shown for the two time points. (B) Shannon diversity index of mice before and after crossover. The data is shown as the mean ± SEM. *P<0.05, **P<0.01, ***P<0.001

determined by Student's t test and adjusted for multiple comparison by Benjamini and Hochberg correction (N=6).

Figure S5. *S. aureus* and *C. bovis* contribute to eczematous inflammation. Related to Figure 5.
(A) Meta-analysis of clinical scores, TEWL and IgE in mice that have been described in Figures 1 and 3. Correlation between relative abundance of 16S rRNA gene sequences of *S. aureus*, *C. bovis* and *C. mastitidis* and TEWL or serum IgE levels in *Adam17*$^{\Delta Sox9}$ and WT mice as determined by Spearman correlation. (B) Correlation between relative abundance of 16S rRNA gene sequences of *S. aureus*, *C. bovis* and *C. mastitidis* and TEWL or clinical score in antibiotics-treated and untreated *Adam17*$^{\Delta Sox9}$ mice as determined by Spearman correlation. (C) Bacterial inoculation protocol. After withdrawal of antibiotic treatment form *Adam17*$^{\Delta Sox9}$ mice that were pretreated with antibiotics, *S. aureus* (SAAS9), *C. bovis* (CBAS9) and *C. mastitidis* (CMAS9) were each inoculated onto the mice (arrows indicate the number of inoculation). (D) Gross phenotype of *Adam17*$^{\Delta Sox9}$ mice that were inoculated with each bacterial strain.

Figure S6. Phenotype of *EGFR*$^{\Delta Sox9}$ mice recapitulates that of *Adam17*$^{\Delta Sox9}$ mice. Related to Figure 6. Gross phenotype of 8-week-old WT and *Egfr*$^{fl/fl}$ *Sox9*-^{Cre} (*Egfr*$^{\Delta Sox9}$) mice.

Figure S7. Occlusive application of *S. aureus* leads to dermatitis formation in WT and *Flg*-/- mice, which is ameliorated in the absence of Langerhans cells. Related to Figure 7. WT, *Flg*$^{-/-}$ and *Flg*$^{-/-}$ Langerin-DTA mice were inoculated with *S. aureus* (SAAS9) via occlusive dressing technique. On day 4 the dressings were removed, and the skin lesions were examined on day 7.

Table S1. Antibiotic sensitivity of *S. aureus* and *Corynebacterium* species isolated from *Adam17*$^{\Delta Sox9}$ mice. Related to Figure 3. Results represent two independent experiments (N=3).

Movie S1. *Adam17*$^{\Delta Sox9}$ mice exhibit strong scratch behavior. Related to Figure 1. A 14 week-old *Adam17*$^{\Delta Sox9}$ mouse is shown. The mouse exhibited continuous scratching behavior that likely reflects strong pruritus.

Table S1

Antibiotics	*S. aureus*	*Corynebacterium* spp
Penicillin	Susceptible	Susceptible
Ampicillin	Susceptible	Susceptible
Cefazolin	Susceptible	Susceptible
Cephalothin	Susceptible	Susceptible
Cefoxitin	Susceptible	Susceptible
Imipenem/cilastatin	Susceptible	Susceptible
Clavulanic acid/amoxicillin	Susceptible	Susceptible
Gentamicin	Susceptible	Susceptible
Amikacin	Susceptible	Susceptible
Spectinomycin	Susceptible	Susceptible
Erythromycin	Susceptible	Susceptible
Lincomycin	Susceptible	Susceptible
Clindamycin	Susceptible	Susceptible
Tetracycline	Susceptible	Susceptible
Chloramphenicol	Susceptible	Susceptible
Sulfamethoxazole-trimethoprim	Susceptible	Susceptible
Enrofloxacin	Susceptible	Susceptible

Supplemental Experimental Procedures

Skin microbiome analysis

Sampling and preparation of DNA

Skin swab samples were obtained from mouse cheek. Extraction and purification of DNA were performed with a protocol adapted from previous studies(Grice et al., 2009; Kong et al., 2012).

Preparation of samples for 454 sequencing

16S rRNA V1-V3 amplicon libraries were prepared from DNA isolated from skin swabs using AccuPrime HF Taq (Invitrogen) and universal primers flanking variable regions V1 (27F, 59-AGAGTTTGATCCTGGCTCAG-39) and V3 (534R, 59-ATTACCGCGGCTGCTGG-39). For each sample, the universal primers were tagged with unique sequences (barcodes) to allow for multiplexing/demultiplexing(Lennon et al., 2010). PCR products were purified with the Agencourt AMPure XP Kit (Beckman Coulter) and quantitated with the Quant-iT dsDNA high-sensitivity assay kit (Invitrogen). Approximately equivalent amounts of each PCR product were then pooled and purified with a Qiagen MinElute column (Qiagen) into 30 mL TE prior to sequencing at the NIH Intramural Sequencing Center. Amplicon libraries were sequenced on a 454 GS FLX (Roche) instrument using titanium chemistry.

Sequence analysis pipeline

Mothur version 1.31.0(Schloss et al., 2009) was used for V1-3 16S rRNA sequence processing, taxonomic classification, definition of operational taxonomic units (OTUs), and calculation of sample diversity. Sequence assembly, filtering, and alignment were performed as described(Grice et al., 2009; Oh et al., 2012). Briefly, sequences matching the human genome were removed (E-value < 0.1) Flowgram data were denoised using the mother implementation of PyroNoise(Quince et al., 2011). Sequences were trimmed of primers and barcodes (primer mismatch ≤1, barcode mismatch ≤2) and filtered for homopolymers ≤8 and length ≥200 bp. Sequences were aligned

using the SILVA ribosomal database(Quast et al., 2013), and then chimera checked using the mothur implementation of UCHIME(Edgar et al., 2011). Sequences were classified using a Ribosomal Database Project naïve Bayesian classifier(Wang et al., 2007). Relative abundance of bacteria at the order and genus level that represented >1% of total 16S rRNA sequences were computed by dividing sequence counts by the total sequences. Finally, custom scripts were generated for taxonomic classifications to the species level for *Staphylococcus* and *Corynebacterium spp.* *Staphylococcus* sequences were speciated aligned to a curated collection of staphylococcal reference sequences from complete genome sequences and type strains. Each sequence was assigned a label based on the consensus call of sequence alignments with the lowest edit distance between a query and reference. *Corynebacterium* sequences were speciated using BLAST on a ≥ 99% identity level.

Diversity of microbial community was calculated based on OTUs, no lane masking was applied. OTUs were defined at 97% similarity using the average neighbor method in mothur. Spurious samples usually representing undetected chimeras were removed by subsampled at the smallest sequence number in a sample (n=107). For alpha and beta diversity statistics, subsampling was iterated 100× yielding up to 99.99% similarity in value. Diversity statistics and proportions were calculated from averaged subsampled data. Alpha diversity was represented by Shannon diversity index, which measures the evenness and richness of a community. Beta diversity was represented by Theta similarity index, which measures the community structure/membership(Yue C. and Clayton K., 2005). No lane masking was applied. To estimate sampling saturation, rarefaction curves were generated for each experiment group (*Adam17*$^{\Delta Sox9}$ Abx, *Adam17*$^{\Delta Sox9}$ No Abx, WT Abx, WT No Abx, crossover treatment).

Statistics for microbiome analysis

Statistical analysis was performed with R software version 3.1 (Vienna, Austria)(R Core, 2012). The null-hypothesis that the samples were drawn from a normally distributed population was tested by Shapiro Wilk test and

Lilliefors test (a Kolmogorov Smirnov test) and visualized with Q-Q plots and histograms. Data on relative abundance and diversity were binned for *Adam17*$^{\Delta Sox9}$ vs. WT and No Abx vs. Abx, as well as for before vs. after crossover. We compared the relative abundance of most common bacteria on the genus and species level and the Shannon diversity between *Adam17*$^{\Delta Sox9}$ mice and WT mice with and without Abx at each sampling time point, as well as between before and after crossover among *Adam17*$^{\Delta Sox9}$ mice. *P-values* were calculated with the parametric Student's t test and the nonparametric Wilcoxon rank sum test, and adjusted for multiple comparison (i.e. multiple sampling time points) by Benjamini Hochberg correction using the p.adjust function in R (method='fdr')(Benjamini and Hochberg, 1995) for both tests. To assess the most significant OTUs contributing to variation in microbial community structure (Theta similarity index) we used the Spearman test. Statistical significance was ascribed to a two-sided alpha level of the adjusted *P*-values ≤0.05. All data are represented as mean ± standard error of the mean unless otherwise indicated.

Supplemental References

Benjamini, Y., and Hochberg, Y. (1995). Controlling the false discovery rate: a practical and powerful approach to multiple testing. J R Stat Soc B (Methodological) *57*, 289-300.

Edgar, R.C., Haas, B.J., Clemente, J.C., Quince, C., and Knight, R. (2011). UCHIME improves sensitivity and speed of chimera detection. Bioinformatics *27*, 2194-2200.

Grice, E.A., Kong, H.H., Conlan, S., Deming, C.B., Davis, J., Young, A.C., Bouffard, G.G., Blakesley, R.W., Murray, P.R., Green, E.D., *et al.* (2009). Topographical and temporal diversity of the human skin microbiome. Science *324*, 1190-1192.

Kong, H.H., Oh, J., Deming, C., Conlan, S., Grice, E.A., Beatson, M.A., Nomicos, E., Polley, E.C., Komarow, H.D., Murray, P.R., *et al.* (2012).

Temporal shifts in the skin microbiome associated with disease flares and treatment in children with atopic dermatitis. Genome Res. *22*, 850-859.

Lennon, N.J., Lintner, R.E., Anderson, S., Alvarez, P., Barry, A., Brockman, W., Daza, R., Erlich, R.L., Giannoukos, G., Green, L.*, et al.* (2010). A scalable, fully automated process for construction of sequence-ready barcoded libraries for 454. Genome biology *11*, R15.

Oh, J., Conlan, S., Polley, E.C., Segre, J.A., and Kong, H.H. (2012). Shifts in human skin and nares microbiota of healthy children and adults. Genome Med. *4*, 77.

Quast, C., Pruesse, E., Yilmaz, P., Gerken, J., Schweer, T., Yarza, P., Peplies, J., and Glockner, F.O. (2013). The SILVA ribosomal RNA gene database project: improved data processing and web-based tools. Nucleic Acids Res *41*, D590-596.

Quince, C., Lanzen, A., Davenport, R.J., and Turnbaugh, P.J. (2011). Removing noise from pyrosequenced amplicons. BMC bioinformatics *12*, 38.

R Core (2012). R: A language and environment for statistical computing. *Vienna, Austria*, http://www.R-project.org/.

Schloss, P.D., Westcott, S.L., Ryabin, T., Hall, J.R., Hartmann, M., Hollister, E.B., Lesniewski, R.A., Oakley, B.B., Parks, D.H., Robinson, C.J.*, et al.* (2009). Introducing mothur: open-source, platform-independent, community-supported software for describing and comparing microbial communities. Appl. Environ. Microbiol. *75*, 7537-7541.

Wang, Q., Garrity, G.M., Tiedje, J.M., and Cole, J.R. (2007). Naive Bayesian classifier for rapid assignment of rRNA sequences into the new bacterial taxonomy. Appl. Environ. Microbiol. *73*, 5261-5267.

Yue C., J., and Clayton K., M. (2005). A similarity measure based on species proportions. Communications in Statistics-theory and Methods *34*, 2123-2131.